LETTER TO THE EDITOR

# B fields in OB stars (BOB): FORS 2 spectropolarimetric follow-up of the two rare rigidly rotating magnetosphere stars HD 23478 and HD 345439\*

S. Hubrig<sup>1</sup>, M. Schöller<sup>2</sup>, L. Fossati<sup>3</sup>, T. Morel<sup>4</sup>, N. Castro<sup>3</sup>, L. M. Oskinova<sup>5</sup>, N. Przybilla<sup>6</sup>, S. S. Eikenberry<sup>7</sup>, M.-F. Nieva<sup>6</sup>, N. Langer<sup>3</sup>, and the BOB collaboration

- <sup>1</sup> Leibniz-Institut für Astrophysik Potsdam (AIP), An der Sternwarte 16, 14482 Potsdam, Germany e-mail: shubrig@aip.de
- <sup>2</sup> European Southern Observatory, Karl-Schwarzschild-Str. 2, 85748 Garching, Germany
- <sup>3</sup> Argelander-Institut für Astronomie, Universität Bonn, Auf dem Hügel 71, 53121 Bonn, Germany
- <sup>4</sup> Institut d'Astrophysique et de Géophysique, Université de Liège, Allée du 6 Août, Bât. B5c, 4000 Liège, Belgium
- <sup>5</sup> Universität Potsdam, Institut für Physik und Astronomie, 14476 Potsdam, Germany
- 6 Institute for Astro- and Particle Physics, University of Innsbruck, Technikerstr. 25/8, 6020 Innsbruck, Austria
- Department of Astronomy, University of Florida, 2011 Bryant Space Center, Gainesville, FL 32611

Received; accepted

#### **ABSTRACT**

Aims. Massive B-type stars with strong magnetic fields and fast rotation are very rare and provide a mystery for theories of both star formation and magnetic field evolution. Only two such stars, called  $\sigma$  Ori E analogs, were previously known. Recently, a team involved in APOGEE, one of the Sloan Digital Sky Survey III programs, announced the discovery of two additional rigidly rotating magnetosphere stars, HD 23478 and HD 345439. The presence of magnetic fields in these newly discovered  $\sigma$  Ori E analogs was not investigated in the past.

*Methods*. In the framework of our ESO Large Programme, and one normal ESO programme, we carried out low-resolution FORS 2 spectropolarimetric observations of HD 23478 and HD 345439.

Results. From the measurements using hydrogen lines, we discover a rather strong longitudinal magnetic field of the order of up to  $1.5 \, \text{kG}$  in HD 23478, and up to  $1.3 \, \text{kG}$  using the entire spectrum. The analysis of HD 345439 using four subsequent spectropolarimetric subexposures does not reveal the presence of a magnetic field at a significance level of  $3\sigma$ . On the other hand, the inspection of individual subexposures indicates that HD 345439 may host a strong magnetic field, rapidly varying over 88 minutes. A hint at the fast rotation of HD 345439 is also given by the behaviour of several metallic and He I lines in the low-resolution FORS 2 spectra, showing profile variations already on such a short time scale.

**Key words.** stars: early-type — stars: fundamental parameters – stars: individual: HD 23478 and HD 345439 – stars: magnetic field – stars: variables: general

## 1. Introduction

The increasing rate of detections of magnetic fields in massive stars during the last years generates a strong motivation to study correlations between evolutionary state, rotation velocity, and surface composition (e.g. Brott et al. 2011; Potter et al. 2012) aiming at understanding the origin and the role of magnetic fields in massive stars. Recent observations indicate that the presence of magnetic fields may be responsible for a wide range of phenomena observed in massive stars, such as chemical peculiarity, periodic UV wind-line variability, cyclic variability in H $\alpha$  and He II  $\lambda$ 4686, excess emission in UV-wind lines, and unusual X-ray emission (e.g. Schnerr et al. 2008; Oskinova et al. 2011a). The variability is likely due to material that is guided by the large-scale magnetic field that corotates with the star (e.g. Groote & Hunger 1982). To properly understand and model all these phenomena, the knowledge of the magnetic field behaviour, i.e.

its configuration, strength, and variability, in massive stars is of utmost importance.

The presence of a rigidly rotating magnetosphere in the early B-type stars HD 23478 and HD 345439 was recently discovered in the Apache Point Observatory Galactic Evolution Experiment (APOGEE; Eikenberry et al. 2014) using highresolution ( $R \sim 22\,500$ ) near-infrared H-band spectra. The authors detected in the APOGEE bandpass prominent Brackett series emission lines with broad double-horned profiles, which are characteristic for the presence of a rigidly rotating magnetosphere (RRM), like found in the prototype star  $\sigma$  Ori E (see their Fig. 4). The strong magnetic field and fast rotation lead to the formation of a centrifugally supported magnetosphere with rotationally modulated hydrogen line emission explained within the RRM model (e.g. Townsend et al. 2005). Among  $\sigma$  Ori E, HD 23478, and HD 345439, the latter appears to display the strongest RRM feature. Eikenberry et al. (2014) report that the optical spectra of HD 23478 and HD 345439 obtained with the Hobby-Eberly-Telescope at a medium resolving power of 18 000 indicate a classification B3IV for the former star and B1V-B2V for the latter. While they determine a v sin i value for HD 23478

<sup>\*</sup> Based on observations obtained in the framework of the ESO Prgs. 191.D-0255(E) and 094.D-0355(B).

of about  $125 \pm 20 \, \mathrm{km \, s^{-1}}$ , HD 345439, in contrast, appears to be one of the fastest known rotators among magnetic main-sequence stars with  $v \sin i \sim 270 \pm 20 \, \mathrm{km \, s^{-1}}$ . Furthermore, the authors report that HD 23478 exhibits a broad H $\alpha$  RRM signature, while for HD 345439 the H $\alpha$  profile shows a slight bump on the red side.

In this work, we present spectropolarimetric follow-up observations of HD 23478 and HD 345439 obtained in the framework of our BOB (B fields in OB stars) collaboration (Morel et al. 2014) using FORS 2 (FOcal Reducer low dispersion Spectrograph) mounted on the 8-m Antu telescope of the VLT. We intend to search for the presence of strong magnetic fields in both stars, which were implicitly detected through the RRM interpretation of their NIR spectra by Eikenberry et al. (2014).

# 2. Magnetic field measurements using FORS 2 spectropolarimetry

Low-resolution FORS 2 observations for HD 23478 and HD 345439 were obtained in 2014 on November 17 and June 2, respectively. FORS 2 is a multi-mode instrument equipped with polarisation analysing optics comprising super-achromatic halfwave and quarter-wave phase retarder plates, and a Wollaston prism with a beam divergence of 22" in standard resolution mode. We employed the GRISM 600B and the narrowest available slit width of 0.4 to obtain a spectral resolving power of  $R \sim 2000$ . The use of the mosaic detector with a pixel size of  $15 \,\mu\text{m}$  allowed us to cover a spectral range from 3250 to 6215 Å, which includes all Balmer lines apart from  $H\alpha$ , and numerous He I lines. For each star, four consecutive observations were obtained with pairs of position angles separated by 90°, namely  $[-45^{\circ}, +45^{\circ}, +45^{\circ}, -45^{\circ}, -45^{\circ}, +45^{\circ}, +45^{\circ}, -45^{\circ}]$ . The exposure time for each position angle was 20 sec for HD 23478, and 600 sec for HD 345439. A peak signal-to-noise ratio (SNR) of 1900 in the final Stokes I spectrum was achieved for HD 23478, while for HD 345439 we obtained a peak SNR of ~900.

The V/I spectrum is calculated using:

$$\frac{V}{I} = \frac{1}{2} \left\{ \left( \frac{f^{o} - f^{e}}{f^{o} + f^{e}} \right)_{-45^{\circ}} - \left( \frac{f^{o} - f^{e}}{f^{o} + f^{e}} \right)_{+45^{\circ}} \right\}$$
(1)

where  $+45^{\circ}$  and  $-45^{\circ}$  indicate the position angle of the retarder waveplate and  $f^{\circ}$  and  $f^{e}$  are the ordinary and extraordinary beams, respectively. Null profiles, N, are calculated as pairwise differences from all available V profiles. From these,  $3\sigma$ -outliers are identified and used to clip the V profiles. This removes spurious signals, which mostly come from cosmic rays, and also reduces the noise. The mean longitudinal magnetic field,  $\langle B_z \rangle$ , is measured on the rectified and clipped spectra based on the relation

$$\frac{V}{I} = -\frac{g_{\text{eff}} e \lambda^2}{4\pi m_e c^2} \frac{1}{I} \frac{dI}{d\lambda} \langle B_z \rangle , \qquad (2)$$

where V is the Stokes parameter that measures the circular polarization, I is the intensity in the unpolarized spectrum,  $g_{\rm eff}$  is the effective Landé factor, e is the electron charge,  $\lambda$  is the wavelength,  $m_{\rm e}$  is the electron mass, e is the speed of light,  ${\rm d}I/{\rm d}\lambda$  is the wavelength derivative of Stokes I, and  $\langle B_{\rm z} \rangle$  is the mean longitudinal (line-of-sight) magnetic field.

The longitudinal magnetic field is usually measured in two ways: using only the hydrogen Balmer lines or using the entire spectrum including all available lines. To identify any systematic differences that could exist in treating the FORS 2 data by

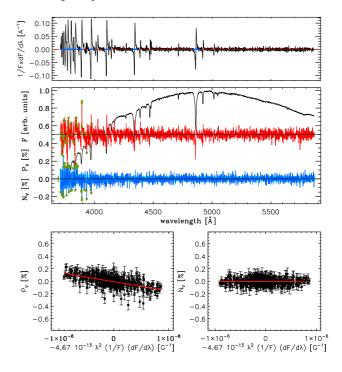


Fig. 1. Graphical output of the IRAF/IDL "Bonn pipeline" obtained from the analysis of the FORS 2 data of HD 23478 considering the hydrogen lines. The top panel presents the derivative of Stokes I. The regions used for the calculation of the magnetic field are marked by a thick blue line centered at zero. In the middle panel, the top spectrum presents the Stokes I spectrum arbitrarily normalised to the highest value, the middle red spectrum corresponds to the Stokes V spectrum (in %), while the bottom blue spectrum is the N spectrum (in %). The green asterisks drawn on the Stokes V and N spectra mark the points which have been removed by the sigma clipping. The pale blue strip drawn behind the N spectrum shows the uncertainty associated with each spectral point. As a double-check of the statistical consistency of the data and uncertainties, the thick green bar on the left side of the N spectrum shows the standard deviation of the N profile. In the bottom-left panel, we present the linear fit used for the determination of the magnetic field value using Stokes V (i.e.  $\langle B_z \rangle$ ). The red solid line shows the best fit. From the linear fit we obtain  $\langle B_z \rangle = -1477 \pm 95$  G. In the bottom-right panel, we present the same as in the bottom-left panel, but for the null profile (i.e.  $\langle N_z \rangle$ ). From the linear fit, we obtain  $\langle N_z \rangle = 30 \pm 64$  G.

different research groups, the mean longitudinal magnetic field,  $\langle B_z \rangle$ , was derived in both stars using independent software packages (one developed in Bonn and the other one in Potsdam). For the first reduction, we used a suite of IRAF (Tody 1993)<sup>1</sup> and IDL routines that follow the technique, recipes, and recommendations by Bagnulo et al. (2002, 2012, 2013)<sup>2</sup>. The determination of the mean longitudinal magnetic field using low-resolution FORS spectropolarimetry with the second software package de-

<sup>&</sup>lt;sup>1</sup> Image Reduction and Analysis Facility (IRAF – http://iraf.noao.edu/) is distributed by the National Optical Astronomy Observatory, which is operated by the Association of Universities for Research in Astronomy (AURA) under cooperative agreement with the National Science Foundation.

<sup>&</sup>lt;sup>2</sup> More details about the applied data reduction and analysis procedure of FORS spectropolarimetric data will be given in a separate work (Fossati et al., in preparation).

**Table 1.** Summary of the results obtained for HD 23478 and HD 345439 from the analysis of the hydrogen lines and of the entire spectrum.

Object	Subexposures	Group	Hydrogen				All			
			$\langle B_{\rm z} \rangle$ [G]	$\sigma_B$	$\langle N_{\rm z} \rangle$ [G]	$\sigma_N$	$\langle B_{\rm z} \rangle$ [G]	$\sigma_{\scriptscriptstyle B}$	$\langle N_{\rm z} \rangle$ [G]	$\sigma_N$
HD 23478	all	Bonn	$-1477 \pm 95$	15.5	30± 64	0.5	$-1302 \pm 59$	21.9	74± 49	1.5
		Potsdam	$-1347\pm114$	11.8	$50 \pm 93$	0.5	$-1139 \pm 84$	13.5	$45 \pm 70$	0.6
HD 345439	all	Bonn	4±121	0.0	23±111	0.2	$-2 \pm 78$	0.0	36± 74	0.5
		Potsdam	57±153	0.4	58±136	0.4	$-22\pm116$	0.2	$64 \pm 103$	0.6
	1+2	Bonn	649±169	3.8	-117±157	0.7	389±105	3.7	104±101	1.0
		Potsdam	638±183	3.5	$-197 \pm 188$	1.0	507±134	3.8	$-93 \pm 143$	0.6
	3+4	Bonn	-618±171	3.6	188±154	1.2	$-375\pm109$	3.4	18±103	0.2
		Potsdam	-574±193	3.0	281±192	1.5	$-501 \pm 146$	3.4	$207 \pm 145$	1.4
	1	Bonn	435±244	1.8			418±159	2.6		
		Potsdam	414±282	1.5			436±212	2.1		
	2	Bonn	631±253	2.5			252±148	1.7		
		Potsdam	789±246	3.2			565±188	3.0		
	3	Bonn	$-509\pm242$	2.1			$-402\pm160$	2.5		
		Potsdam	$-303\pm282$	1.1			$-298\pm212$	1.4		
	4	Bonn	-1181±328	3.6			-534±166	3.2		
		Potsdam	$-840\pm262$	3.2			$-689 \pm 198$	3.5		

veloped in Potsdam is described by Hubrig et al. (2014, 2015) and by Schöller et al. (in preparation). In general, the measurement method is the same for both pipelines. A few minor differences refer to the clipping procedure, rectification, and the choice of the wavelength regions including the hydrogen lines. Furthermore, Monte Carlo bootstrapping tests are carried out in the second software package (e.g. Rivinius et al. 2010). In these tests, we generate 250 000 statistical variations of the original dataset by the bootstrapping technique, and analyze the resulting distribution  $P(\langle B_z \rangle)$  of the regression results. Mean and standard deviation of this distribution are identified with the most likely mean longitudinal magnetic field and its 1  $\sigma$  error, respectively. The main advantage of this method is that it provides an independent error estimate. The measurement uncertainties for both stars obtained before and after Monte Carlo bootstrapping tests were found to be in close agreement, indicating the robustness of the measurement method.

The results of the magnetic field measurements carried out using independent reduction and measurement packages are listed in Table 1. For the first software package developed in Bonn, the uncertainty on the  $\langle B_z \rangle$  and  $\langle N_z \rangle$  values is the  $\chi^2$ -scaled uncertainty (Bagnulo et al. 2012), while the uncertainty determined by the second software package developed in Potsdam involves in addition the bootstrapping results. In each column, the numbers  $\sigma_B$  and  $\sigma_N$  after the  $\langle B_z \rangle$  and  $\langle N_z \rangle$  values refer to the sigma detection.

A strong magnetic field at a significance level of more than  $10\sigma$  was achieved for HD 23478 using the hydrogen lines and the entire spectrum. Using the first software package we obtain  $\langle B_z \rangle = -1302 \pm 59\,\mathrm{G}$  for the whole spectrum and  $\langle B_z \rangle_{\mathrm{hyd}} = -1477 \pm 95\,\mathrm{G}$ , while using the second software package we measure  $\langle B_z \rangle = -1139 \pm 84\,\mathrm{G}$  and  $\langle B_z \rangle_{\mathrm{hyd}} = -1347 \pm 114\,\mathrm{G}$ . For both reduction packages the magnetic field values obtained for each pair of position angles separated by 90° show negative polarity, are all consistent with each other, and are of similar order. No significant fields were detected in the null spectra calculated by combining the subexposures in such a way that the intrinsic source polarization cancels out, yielding a diagnostic null N spectrum. Figure 1 presents the main graphical output of the "Bonn pipeline" showing the clear magnetic field detection obtained form the analysis of the hydrogen lines of HD 23478.

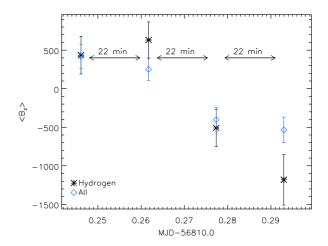


**Fig. 2.** Variation of the  $\langle B_z \rangle$  value obtained for HD 345439 from the analysis of the hydrogen lines (black asterisks) and of the whole spectrum (blue rhombs). Between each point there is a time span of about 22 min.

In the analysis of HD 345439, using four consecutive observations obtained with pairs of position angles separated by 90°, we obtained a clear non-detection, which is presented in the second line in Table 1. However, after splitting the observations into two data sets, i.e. using the first two pairs and the second two pairs consisting of observations at the retarder waveplate positions  $[-45^{\circ}, +45^{\circ}, +45^{\circ}, -45^{\circ}]$ , we obtain 3.0 to 3.8 $\sigma$  detections shown in the third and fourth lines of the table. The fact that the first and second data-sets led to opposite  $\langle B_z \rangle$  values, though almost equal in modulus, led to a non-detection in the measurements using the whole available data set. This behaviour might be suggestive of a very fast rotating star with a magnetic field axis inclined relative to the rotation axis. Given the apparent fast and large variation of the value of the longitudinal magnetic field, we then decided to measure the magnetic field using each individual pair obtained at the retarder waveplate positions  $[-45^{\circ}, +45^{\circ}]$  and separated by roughly 22 minutes. The results are presented in the last four lines of Table 1. In this case, the null profile can not be extracted, since the measurements were

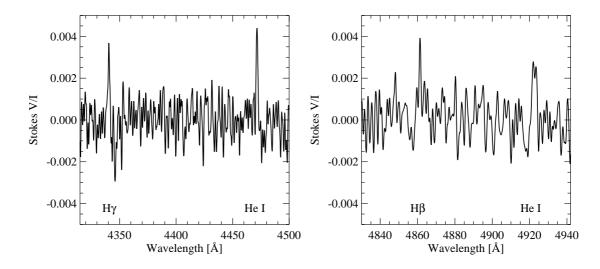


**Fig. 3.** Left-side panel: Stokes V spectrum of HD 345439 in the vicinity of H $\gamma$  and He I  $\lambda$ 4471 obtained from the combination of the first two pairs of subexposures. The shape of the Zeeman features indicates the presence of a longitudinal magnetic field of positive polarity. Right-side panel: Stokes V spectrum of HD 345439 in the vicinity of H $\beta$  and He I  $\lambda$ 4922 lines obtained from the combination of the last two pairs of subexposures. The shape of the Zeeman features indicates the presence of a longitudinal magnetic field of negative polarity.

done using observations at just two position angles. Note also that no sigma clipping was adopted for this specific analysis, because the sigma clipping is applied on the basis of the null profile. Figure 2 shows the variation of the  $\langle B_z \rangle$  value obtained from the analysis of the hydrogen lines and of the entire spectrum using the first software package developed in Bonn. We discover that the mean longitudinal magnetic field measured on hydrogen lines is changing from about +500 G measured in the first pair of subexposures to about -1200G measured in the last pair of subexposures. Using the second software package developed in Potsdam we obtained similar magnetic field behaviour, but with somewhat different absolute values of the field. The detections are achieved at a significance level of 3 to  $3.6\sigma$  in two subexposures. In Figure 3, we present Stokes V spectra obtained for the combinations of the first two pairs of subexposures and for the last two pairs of subexposures in the vicinity of the hydrogen and He I lines. The different shape of the Zeeman features indicates that the magnetic field polarity has changed after the the second subexposure. We note that all tests we performed on the data did not give an indication of the presence of relevant systematic noise. Nevertheless, it is important to obtain in the future more spectropolarimetric data to confirm this behaviour.

An indication for the fast rotation of HD 345439 is also given by the behaviour of several metallic and He I lines in the low-resolution FORS 2 spectra, showing profile variations already on a time scale of 88 min. In Fig. 4, we present the behaviour of the Si III  $\lambda$ 4553 and the He I  $\lambda$ 4388 and He I  $\lambda$ 4471 lines in the FORS 2 Stokes *I* spectra obtained for each pair of subexposures recorded with a time lapse of 22 min. The profile of the Si III line becomes asymmetric in the last pair of subexposures, i.e. at the time when we observe negative field polarity. We note, however, that the level of variability of the Si III  $\lambda$ 4553 line profile is not significantly higher than that in neighbouring continuum regions. On the other hand, similar asymmetric profiles of Si lines are detected in our FEROS (Fiber-fed Extended Range Optical Spectrograph) spectrum of  $\sigma$  Ori E obtained in the framework of the ESO programme 091.C-0713(A). As for the behaviour of the

He I  $\lambda$ 4388 and He I  $\lambda$ 4471 lines, their intensity is lower at the phase when the polarity of the field is positive and it becomes higher when the field is negative. Such a fast spectral and longitudinal magnetic field variability suggests that the rotation period should be very short, probably less than one day. The rapid change in the strength of the mean longitudinal magnetic field by about 1 kG over 88 min in HD 345439 is reminiscent of the mean longitudinal magnetic field behaviour in the fast rotating  $\sigma$  Ori E analog HR 7355 with a rotation period of 0.52 d. This star shows a field variation of about 1 kG within a phase interval of 0.1, corresponding to 75 min (see Fig. 3 in Rivinius et al. 2013). Therefore, it is not impossible that the rotation period of HD 345439 is also significantly shorter than one day.

No spectral variability was detected in the eight low-resolution FORS 2 spectra for HD 23478 taken within 15 min. This star was intensively studied photometrically by Jerzykiewicz (1993), who suggested a photometric/rotation period of 1.05 d and, using a radius estimated from the spectral type, obtained 240 km s<sup>-1</sup> for the equatorial rotation velocity.

### 3. Discussion

Our spectropolarimetric follow-up of the early B-type stars HD 23478 and HD 345439, with recently discovered rigidly rotating magnetospheres, using FORS 2 observations, reveals the presence of a strong longitudinal magnetic field of the order of 1.5 kG in HD 23478. We also found an indication for the presence of a rapidly changing magnetic field in the fast rotator HD 345439. Obviously, additional follow-up spectropolarimetric monitoring of the behaviour of the magnetic field in HD 23478 and HD 345439 is urgently needed to confirm and characterize the magnetic field topology of both stars. Knowledge of the structure of the magnetic field is of crucial importance for the understanding of the nature of these stars belonging to the group of  $\sigma$  Ori E analogs.

This type of stars is extremely rare: apart from  $\sigma$  Ori E (e.g. Groote & Hunger 1997), only two other stars, HR 5907 and

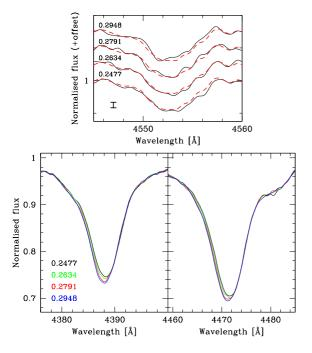


**Fig. 4.** Line profile variability of Si and He in the FORS 2 Stokes *I* spectra of HD 345439 obtained for each pair of subexposures, i.e. with a time lapse of 22 min. Top panel presents the behaviour of the Si III  $\lambda$ 4553 line. The mean profile is indicated by the red dashed line. The numbers close to the plotted line profiles refer to the time of the observation calculated as MJD-56810. The vertical bar on the left side shows the noise level. In the bottom panel we present overplotted profiles of the He I  $\lambda$ 4388 and He I  $\lambda$ 4471 lines. Their intensity is lower at the phase when the polarity of the field is positive and it becomes higher when the field is negative. The error bar is too small to be presented in these plots.

HR 7355, are known to belong to this group called the  $\sigma$  Ori E analogs (Grunhut et al. 2012; Rivinius et al. 2013). Their very strong magnetic fields and extraordinary fast rotation provide a mystery for theories of both star formation and magnetic field evolution. Both stars have similar dipole strengths of the order of 10 kG and similar very short half-day rotation periods. However, the spindown timescale via magnetic braking is expected to be much shorter than their estimated ages (e.g., Rivinius et al. 2013; Mikulášek et al. 2010).

The emission variability in hydrogen lines in the  $\sigma$  Ori E analogs suggests that gas is trapped in magnetospheric clouds. The high strength of the magnetic fields controlling the stellar winds and fast rotation makes these type of stars a test case for models of X-ray production. Only low resolution X-ray spectra were so far measured for three members of this group,  $\sigma$  Ori E, HR 5907, and HR 7355 (e.g., Petit et al. 2013; Nazé et al. 2014). We retrieved and analyzed these archival XMM-Newton and Chandra observations using most recent calibrations. Our analysis of the X-ray spectra of HR 5907 and HR 7355 shows that these stars are even harder X-ray sources than  $\sigma$  Ori E; e.g., the emission measure weighted temperature of the hot plasma in HR 5907 is 80 MK, and in HR 7355 it is 60 MK. Given that the winds in magnetic B-type dwarf stars are weak, with velocities not exceeding a few hundred km s<sup>-1</sup> (Oskinova et al. 2011b), it is very difficult to explain such high temperatures in the framework of the magnetically confined wind shock model (Babel &

Montmerle 1997). On the other hand, non-thermal emission can be expected from stars with strong magnetic fields (Leto et al. 2006). Our analysis of archival data showed that the presence of non-thermal radiation in these objects is very likely (Oskinova et al., in preparation). New, already approved *XMM-Newton* observations of HD 345439 will probe whether hard non-thermal X-rays are present in this object and shed new light on the mechanisms of X-ray generation in strongly magnetic fast rotators.

Acknowledgements. TM acknowledges financial support from Belspo for contract PRODEX GAIA-DPAC. LF acknowledges financial support from the Alexander von Humboldt Foundation. LMO thanks DLR grant 50 OR 1302. The authors thank to Rainer Arl, Artemio Herrero, and Fabian Schneider for useful comments.

References Babel, J. & Montmerle, T. 1997, A&A, 323, 121 Bagnulo, S., Szeifert, T., Wade, G. A., et al. 2002, A&A, 389, 191 Bagnulo, S., Landstreet, J. D., Fossati, L. & Kochukhov, O. 2012, A&A, 538, A129 Bagnulo, S., Fossati, L., Kochukhov, O. & Landstreet, J. D. 2013, A&A, 559, A103 Brott, I., Evans, C. J., Hunter, I., et al. 2011, A&A, 530, A116 Eikenberry, S. S., Chojnowski, S. D., Wisniewski, J., et al. 2014, ApJL, 784, L30 Groote, D., & Hunger, K. 1982, A&A, 116, 64 Groote, D., & Hunger, K. 1997, A&A, 319, 250 Grunhut, J. H., Rivinius, Th., Wade, G. A., et al. 2012, MNRAS, 419, 1610 Hubrig, S., Schöller, M., & Kholtygin, A. F. 2014, MNRAS, 440, 1779 Hubrig, S., Schöller, M., Kholtygin, A. F., et al. 2015, MNRAS, 447, 1885 Jerzykiewicz, M. 1993, A&AS, 97, 421 Leto, P., Trigilio, C., Buemi, C. S., et al. 2006, A&A, 458, 831 Mikulášek, Z., Krtička, J., Henry, G. W., et al. 2010, A&A, 511, L7 Morel, T., Castro, N., Fossati, L., et al. 2014, Msngr. 157, 27 Nazé, Y., Petit, V., Rinbrand, M., et al. 2014, ApJS, 215, 10 Oskinova, L. M., Hamann, W.-R., Cassinelli, J. P., et al. 2011a, AN, 332, 988 Oskinova, L. M., Todt, H., Ignace, R., et al. 2011b, MNRAS, 416, 1456 Petit, V., Owocki, S. P., Wade, G. A., et al. 2013, MNRAS, 429, 398 Potter, A. T., Chitre, S. M., Tout, C. A. 2012, MNRAS, 424, 2358 Rivinius, T., Szeifert, T., Barrera, L., et al. 2010, MNRAS, 405, L46 Rivinius, T., Townsend, R. H. D., Kochukhov, O., et al. 2013, MNRAS, 429, 177 Schnerr, R. S., Henrichs, H. F., Neiner, C., et al. 2008, A&A, 483, 857 Tody, D. 1993, in Astronomical Data Analysis Software and Systems II, ed. R. J. Hanisch, R. J. V. Brissenden, & J. Barnes (San Francisco: ASP), ASP Conf. Ser., 52, 173 Townsend, R. H. D., Owocki, S. P., & Groote, D. 2005, ApJ, 630, L81